A normalization-based approach to the mobility analysis of spatial compliant multi-beam modules[1]

Guangbo Hao[a], Xianwen Kong[b, 2]

[a]*Department of Electrical and Electronic Engineering, School of Engineering, University College Cork, Cork, Ireland*
[b]*School of Engineering and Physical Sciences, Heriot-Watt University, Edinburgh, EH14 4AS, UK*

ABSTRACT

This paper presents a normalization-based approach to the mobility analysis of spatial compliant multi-beam modules to address the dimensional-inhomogeneity issue of motion/load. Firstly, two spatial non-tilted and tilted multi-beam modules, composed of uniform beams with symmetrical cross sections and same length, are proposed. Using a normalization technique, the compliance matrices of these spatial multi-beam modules are derived, from which the DOF (degrees-of-freedom) of the compliant modules can be obtained by direct observation and/or screw representation. The results are compared with those obtained without normalization. It is shown that the DOF of these compliant modules can be identified more easily using the proposed approach than the approach without normalization. Then, two spatial double non-tilted and tilted three-beam modules are proposed and analyzed for potential applications such as acting as building blocks of new compliant manipulators. The normalization-based approach can also be used for the mobility analysis of spatial compliant multi-sheet modules such as the parallelogram module and the four-sheet rotational module and the error analysis of spatial multi-beam modules with beams of compatible length.

Keywords: Compliant Mechanisms; Spatial Modules; Mobility Analysis; Normalization

1. Introduction

Compliant mechanisms [1, 2], transmitting motion/loads by the deformation of compliant members, have many potential merits such as zero backlashes, no need for lubrication, reduced friction and wear, and high precision compared with traditional rigid-body mechanisms [3, 4]. They can be used in a variety of applications, especially where high-precision motions are required, such as precision motion positioning stages, precision robotics in biomedical applications, MEMS sensors and actuators, amplifiers, grippers, adaptive mechanisms, and design-for-no-assembly [5–10]. The degrees-of-freedom (DOF) of traditional rigid-body mechanisms can be identified and calculated using formulas proposed in the literatures. But for the compliant mechanisms, there is no apparent boundary to identify the DOF or the degrees-of-constraint (DOC) due to complex issues such as dimension, loads and motion range. In [11], the DOF of compliant mechanisms, especially planar compliant mechanisms, were determined using the Pseudo-Rigid-Body-Model concept. References [12, 13] proposed an eigenscrew-based method to determine the DOF or compliance of compliant mechanisms. In addition, the constraint-based design approach (CBDA) [14], the screw theory based approach (STBA) [15] and the freedom and constraint topology approach (FACT) [16, 17] have been proposed to analyze the DOF and/or DOC of compliant mechanisms. Different from the CBDA, the STBA uses the mathematical expressions to represent the CBDA, and the FACT employs the geometric figures to visualize the CBDA. The STBA and FACT can also be used to synthesize the screw motion.

In analyzing the DOF of a compliant mechanism quantitatively, we need to compare the output displacements to identify the DOF/DOC. If one displacement is much larger than another displacement under the same dimension, then the larger one can be regarded as the DOF. However, if two displacements, such as one translational displacement and one rotational angle, are not under the same dimension, then the DOF identification becomes difficult.

In addition, the DOF of certain compliant mechanisms, such as the linear motion flexure [1, 5] composed of two parallelogram modules in mirror-symmetry, can also degenerate into the DOC when they achieve a large range of motion. This is caused by the significant load-stiffening effect [1, 18]. Under the small deflection assumption, this issue can be neglected. It should also be noted that the location and magnitude of applied loads may affect the identification of the DOF and DOC. For example, for a cantilever beam, it is well known that the axial displacement of the tip is usually thought to be the DOC, while the transverse displacement of the tip is usually regarded as the DOF. However, if the axial force acting at the tip of the beam was much larger than the exerted transverse force, the resulting axial displacement would be much larger than the transverse displacement.

In order to make translational displacements and rotational angles (or the forces and the moments) comparable, a normalization strategy (non-dimensional/homogeneous measures) is needed to unify the dimensions of compliant mechanisms. A normalization technique has been employed in the modeling and design of compliant/flexural mechanisms [5, 18–23]. It has been shown that the normalization strategy can simplify equations and derivation in the analysis of compliant mechanisms. In rigid-body manipulators/mechanisms, such strategy has also been employed. For example, Ref. [24] proposed a characteristic length for normalizing the Jacobin matrix of rigid-body robots. The normalization technique [5, 18–23] provides a way to deal with the above non-homogeneous issue in identifying the DOF of compliant mechanisms. In addition, in the analysis of compliant mechanisms, one can assume that all loads are in the same order of magnitude and comparable under the same dimension.

---

[1]Part of this paper was presented in the 13th World Congress in Mechanism and Machine Science, June 19-25, 2011, Guanajuato, Mexico. A23-390.
[2]Corresponding author. Email: X.Kong@hw.ac.uk. Tel: +44(0)1314513688.

Based on the above advances, this paper aims to present a normalization-based approach to the mobility analysis of a class of spatial compliant parallel modules[3] (CPMs) with distributed compliance in order to identify the DOF from the normalized compliance matrices in a straightforward manner. This class of spatial CPMs are composed of uniform beams with generic cross-sections (such as symmetrical and rectangular) and the same length or compatible length at least, which can be used in many applications either independently or as a compositional unit of a complaint manipulator [21, 22]. This paper mainly focuses on the mobility analysis of typical spatial multi-beam modules with beams of *symmetrical* cross-sections and *same* length to demonstrate the normalization-based approach. We will discuss two types of typical spatial multi-beam modules: non-tilted multi-beam modules (all identical beams are parallel and spaced uniformly around a circle on the base and the motion stage to produce planar motion) and tilted multi-beam modules (the axes of all the identical beams intersect at a point and the beams are uniformly spaced around two circles on the motion stage and base to produce spherical motion). For the spatial multi-sheet modules with beams of rectangular cross-sections such as the parallelogram module and the four-sheet rotational module, the mobility analysis using the proposed normalization-based approach is briefly discussed in Appendices A and B in order to avoid the analogous tedious derivations. For the spatial multi-beam modules with beams of compatible length, a typical case is the error analysis, which can be found in Appendix C using the proposed method. It is noted that if beams in a spatial CPM have significantly different length, compared with the long beam(s), a shorter beam will degrade to a 3-DOF lumped-compliance spherical joint or even a DOC from a 5-DOF compliant mechanism, which is out of scope of this paper.

This paper is organized as follows. Section 2 recalls the normalization strategy by normalizing the force-displacement equations for a symmetrical cantilever beam. In Section 3, spatial non-tilted multi-beam modules including a spatial three-beam module (TBM) and a spatial double TBM are analyzed using the proposed normalization-based method. Section 4 discusses spatial tilted multi-beam modules including a spatial tilted TBM and a spatial double tilted TBM, Finally, conclusions are drawn.

2. Normalization strategy

The beam-based modules can be normalized as follows [21, 22]. All translational displacements and length parameters are divided by the beam length L, forces by EI/L^2, and moments by EI/L. Here, E and I denote, respectively, the Young's modulus and the second moment of the area of a symmetrical cross-section. $I=\pi D^4/64$ for beams with round cross-section of a diameter D and $I=T^4/12$ for beams with square cross-section of a thickness of T. The normalized beam is equivalent to a beam with unit length, unit Young's modulus and unit cross-sectional moment. Throughout this paper, non-dimensional quantities are represented by the corresponding lower-case letters.

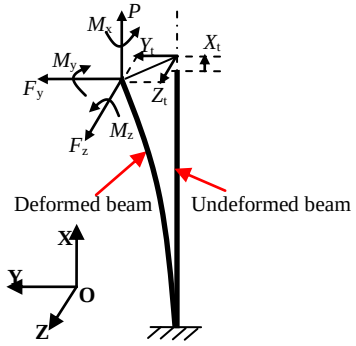

Fig. 1. A basic cantilever beam

For the basic cantilever beam (Fig. 1), P, F_y, F_z, M_x, M_y and M_z denote the actual loads acting at the centre of the free-end to cause motion. P, F_y and F_z are the forces along the X-, Y- and Z-axes, respectively, and M_x, M_y and M_z are the actual moments about the X-, Y- and Z-axes, respectively. X_t, Y_t and Z_t are the translational displacements of the centre of the free-end along X-, Y- and Z-axes, respectively; θ_{tx}, θ_{ty} and θ_{tz} are the rotational displacements of the free-end about the X-, Y- and Z-axes, respectively.

The linear load-displacement equations of the free-end centre without normalization, similar to the ones used in [25, 26], are

$$\begin{bmatrix} P \\ F_y \\ F_z \\ M_x \\ M_y \\ M_z \end{bmatrix} = \begin{bmatrix} \frac{E\pi D^2}{4L}\left(\text{or}\ \frac{ET^2}{L}\right) & 0 & 0 & 0 & 0 & 0 \\ 0 & \frac{12EI}{L^3} & 0 & 0 & 0 & \frac{-6EI}{L^2} \\ 0 & 0 & \frac{12EI}{L^3} & 0 & \frac{6EI}{L^2} & 0 \\ 0 & 0 & 0 & \frac{2GI}{L} & 0 & 0 \\ 0 & 0 & \frac{6EI}{L^2} & 0 & \frac{4EI}{L} & 0 \\ 0 & \frac{-6EI}{L^2} & 0 & 0 & 0 & \frac{4EI}{L} \end{bmatrix} \begin{bmatrix} X_t \\ Y_t \\ Z_t \\ \theta_{tx} \\ \theta_{ty} \\ \theta_{tz} \end{bmatrix} \quad (1)$$

[3] A spatial compliant module/mechanism is a compliant mechanism that has compatible size in three dimensions

where G denotes the shear modulus of material. The entry in the first row and first column is $E\pi D^2/(4L)$ for round beams or ET^2/L for square beams.

Using the above normalization procedure, Eq. (1) can be re-written in a normalized form as:

$$\begin{bmatrix} p \\ f_y \\ f_z \\ m_x \\ m_y \\ m_z \end{bmatrix} = \mathbf{K} \begin{bmatrix} x_t \\ y_t \\ z_t \\ \theta_{tx} \\ \theta_{ty} \\ \theta_{tz} \end{bmatrix} = \begin{bmatrix} d & 0 & 0 & 0 & 0 & 0 \\ 0 & a & 0 & 0 & 0 & c \\ 0 & 0 & a & 0 & -c & 0 \\ 0 & 0 & 0 & \delta & 0 & 0 \\ 0 & 0 & -c & 0 & b & 0 \\ 0 & c & 0 & 0 & 0 & b \end{bmatrix} \begin{bmatrix} x_t \\ y_t \\ z_t \\ \theta_{tx} \\ \theta_{ty} \\ \theta_{tz} \end{bmatrix} \tag{2}$$

where all the loads and displacements are the normalized quantities (scalar) which are corresponding to the non-normalized loads and displacements in Eq. (1). All the non-dimensional numbers, a=12, c=−6, d=16/$(D/L)^2$ for round beams or d=12/$(T/L)^2$ for square beams, b=4, and δ=2G/E=1/(1+ν) (ν is the Poisson ratio of material), are characteristics of the uniform symmetrical beam.

Equation (2), the linear load-displacement equations of a beam, will be used for the mobility analysis of spatial multi-beam modules under small deflection condition that usually assumes the normalized displacements to be less than 0.1 [27]. It should be noted that the smaller the motion range is, the more accurate the linear modeling is.

3. Spatial non-tilted multi-beam modules

In this section, we will further recall the modeling of compliance matrices of a spatial TBM and a spatial double TBM [21] and then analyze their DOF.

3.1. Analysis of a spatial TBM

A spatial TBM [1, 5, 21, 27] is shown in Fig. 2. It is composed of three parts: a base, three parallel beams with symmetrical cross sections and a thin motion stage. The base and motion stage are connected by the three beams. The three beams are spaced uniformly around a circle of a radius r_3 on the base and on the motion stage. The external loads acting on the motion stage cause the motion stage to move through deformation of the beams.

In the initial configuration, a mobile rigid body coordinate system O'-X'Y'Z' and a global fixed coordinate system O-XYZ are coincident and both origins are at the centre, O', of the bottom-plane of the motion stage. All external applied loads, p (axial force), f_y, f_z (transverse forces), m_x (torque), m_y and m_z (bending moments), can be regarded to act at the centre, O', of the motion stage since all forces acting at other points can be transformed to the centre plus extra moments. All translational displacements of the centre, O', along the X-, Y- and Z-axes are denoted by x_s (axial displacement) y_s and z_s (transverse displacements), respectively; All rotational displacements (angles) of the motion stage about the X-, Y- and Z-axes are denoted by θ_{sx} (torsional angle), θ_{sy} and θ_{sz} (bending angles), respectively. All the loads and displacements shown in all the following figures are represented by the nondimensional quantities in the coordinate system O-XYZ.

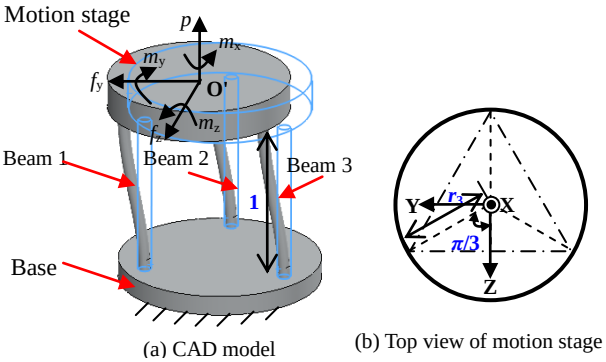

(a) CAD model (b) Top view of motion stage

Fig. 2. A spatial TBM in deformation

In terms of the type synthesis of CPMs in [5, 28], the three out-of-plane DOF, x_s, θ_{sy} and θ_{sz}, of the spatial TBM are suppressed, and the motion stage is constrained to move within the YZ plane, which leaves y_s, z_s and θ_{sx} as the DOF. If the pitch radius r_3 of the beams (hence the motion stage) becomes relatively large, the rotation about the X-axis will be constrained as well. The detailed quantitative analysis of the spatial TBM can be presented in the subsequent sections.

3.1.1. Modeling of the spatial TBM

The modeling of a spatial TBM can refer to the stiffness modeling of compliant parallel structure [21, 29]. The derivations of the linear analysis for the spatial TBM are summarized as follows.

Under the assumption of small rotation angles, the contribution of the rotation order of three Euler angles may be disregarded [30]. By neglecting high order terms of rotational angles in the product of three rotation matrices, the geometry compatibility

conditions, between the mobile end, connected to the motion stage, of each beam and the motion stage, can be expressed in a matrix form as

$$\begin{bmatrix} x_i \\ y_i \\ z_i \\ \theta_{ix} \\ \theta_{iy} \\ \theta_{iz} \end{bmatrix} = \mathbf{D}_{pi} \begin{bmatrix} x_s \\ y_s \\ z_s \\ \theta_{sx} \\ \theta_{sy} \\ \theta_{sz} \end{bmatrix} = \begin{bmatrix} 1 & 0 & 0 & 0 & z_i' & -y_i' \\ 0 & 1 & 0 & -z_i' & 0 & x_i' \\ 0 & 0 & 1 & y_i' & -x_i' & 0 \\ 0 & 0 & 0 & 1 & 0 & 0 \\ 0 & 0 & 0 & 0 & 1 & 0 \\ 0 & 0 & 0 & 0 & 0 & 1 \end{bmatrix} \begin{bmatrix} x_s \\ y_s \\ z_s \\ \theta_{sx} \\ \theta_{sy} \\ \theta_{sz} \end{bmatrix} \tag{3}$$

where $\mathbf{D}_{pi}$ is the transformation matrix of the displacements of the motion stage. x_i, y_i and z_i (i=1, 2, 3) are the translational displacements of the centre (tip) of the mobile end of the i-th beam along the X-, Y- and Z-axes, respectively; θ_{ix}, θ_{iy} and θ_{iz} are the rotational displacements of the mobile end of the i-th beam about the X-, Y- and Z-axes, respectively. x_i', y_i' and z_i' (i=1, 2, 3) are the local coordinates of the tip of the i-th beam relative to mobile rigid body coordinate system ($x_1'=0$, $y_1'=r_3\sin(\pi/3)$, $z_1'=r_3\cos(\pi/3)$ for the tip 1, $x_2'=0$, $y_2'=0$, $z_2'=-r_3$ for the tip 2, $x_3'=0$, $y_3'=-r_3\sin(\pi/3)$, $z_3'=r_3\cos(\pi/3)$ for the tip 3).

Based on Eq. (2), the load-displacements equations for the tip of the i-th beam in the spatial TBM can be obtained as

$$\left[p_i,\, f_{iy},\, f_{iz},\, m_{ix},\, m_{iy},\, m_{iz}\right]^{\mathrm{T}} = \mathbf{K}_i \left[x_i, y_i, z_i, \theta_{ix}, \theta_{iy}, \theta_{iz}\right]^{\mathrm{T}} \tag{4}$$

where $\mathbf{K}_i$=$\mathbf{K}$ (Eq. (2)) is the stiffness matrix for each beam. p_i, f_{iy}, f_{iz}, m_{ix}, m_{iy} and m_{iz} (i=1, 2, 3), denote the internal loads acting at the tip of the i-th beam, of which p_i, f_{iy} and f_{iz} are the forces along the X-, Y- and Z-axes, respectively, and m_{ix}, m_{iy} and m_{iz} are the moments about the X-, Y- and Z-axes, respectively.

Using the transformation matrix $\mathbf{D}_{pi}$ in Eq. (3), the load-equilibrium conditions for the motion stage are shown as follows.

$$\begin{bmatrix} p \\ f_y \\ f_z \\ m_x \\ m_y \\ m_z \end{bmatrix} = \sum_{i=1}^{n=3} \mathbf{D}_{pi}^{\mathrm{T}} \begin{bmatrix} p_i \\ f_{iy} \\ f_{iz} \\ m_{ix} \\ m_{iy} \\ m_{iz} \end{bmatrix} = \sum_{i=1}^{n=3} \begin{bmatrix} 1 & 0 & 0 & 0 & 0 & 0 \\ 0 & 1 & 0 & 0 & 0 & 0 \\ 0 & 0 & 1 & 0 & 0 & 0 \\ 0 & -z_i' & y_i' & 1 & 0 & 0 \\ z_i' & 0 & 0 & 0 & 1 & 0 \\ -y_i' & 0 & 0 & 0 & 0 & 1 \end{bmatrix} \begin{bmatrix} p_i \\ f_{iy} \\ f_{iz} \\ m_{ix} \\ m_{iy} \\ m_{iz} \end{bmatrix} \tag{5}$$

where $\mathbf{D}_{pi}^{\mathrm{T}}$ may be thought of as the transformation matrix of the loads.

Substituting Eq. (4) into Eq. (5), and then substituting Eq. (3) into the result, we have

$$\mathbf{F} = \mathbf{K}_p \mathbf{X}_s \tag{6}$$

where $\mathbf{X}_s = [x_s, y_s, z_s, \theta_{sx}, \theta_{sy}, \theta_{sz}]^{\mathrm{T}}$ and $\mathbf{F} = [p,\, f_y,\, f_z, m_x, m_y, m_z]^{\mathrm{T}}$. $\mathbf{K}_p = \mathbf{D}_{p1}^{\mathrm{T}}\mathbf{K}_1\mathbf{D}_{p1} + \mathbf{D}_{p2}^{\mathrm{T}}\mathbf{K}_2\mathbf{D}_{p2} + \mathbf{D}_{p3}^{\mathrm{T}}\mathbf{K}_3\mathbf{D}_{p3}$, which is the stiffness matrix of the spatial TBM.

The load-displacement relationships for the motion stage can also be re-expressed as

$$\mathbf{X}_s = \mathbf{C}_p \mathbf{F} \tag{7}$$

where $\mathbf{C}_p = \mathbf{K}_p^{-1}$, which is the compliance matrix of the spatial TBM.

Equations (7) and (6) are the forward load-displacement equations and inverse load-displacement equations of the motion stage of the spatial TBM, respectively.

Let the spatial TBM be made of a standard aluminium alloy for which Young's modulus, E, is 69,000 Nmm^{-2} and Poisson's ratio, v, is 0.33. Substituting all the values of the non-dimensional numbers and local coordinates into the compliance matrix in Eq. (7), we have

$$\mathbf{C}_p = \begin{bmatrix} 1/3d & 0 & 0 & 0 & 0 & 0 \\ 0 & \left[\dfrac{(r_3^2 d + 8)}{36(r_3^2 d + 2)}\right] & 0 & 0 & 0 & \dfrac{1}{3(r_3^2 d + 2)} \\ 0 & 0 & \left[\dfrac{(r_3^2 d + 8)}{36(r_3^2 d + 2)}\right] & 0 & \dfrac{-1}{3(r_3^2 d + 2)} & 0 \\ 0 & 0 & 0 & \left[\dfrac{625}{9(2500 r_3^2 + 157)}\right] & 0 & 0 \\ 0 & 0 & \dfrac{-1}{3(r_3^2 d + 2)} & 0 & \dfrac{2}{3(r_3^2 d + 2)} & 0 \\ 0 & \dfrac{1}{3(r_3^2 d + 2)} & 0 & 0 & 0 & \dfrac{2}{3(r_3^2 d + 2)} \end{bmatrix} \tag{8}$$

where $d \geq 10000$ for $L/D \geq 25$ or $L/T > 29$, and r_3 should usually be comparable with the beam length L, which may be larger than 0.5. Note that this compliance matrix is a symmetrical matrix. Under large d, the highlighted diagonal compliance entries (elements (2, 2), (3, 3) and (4, 4)) associated with the two transverse displacements and the torsional angle are much larger than those compliance entries associated with the axial displacement and the two bending angles, and therefore are the dominant entries in the compliance matrix. Equation (8) also captures how the size parameters r_3 and d influence the compliance matrix. If d or r_3 increases, the three rotational angles all decrease.

Equation (8) further shows that θ_{sz}=0 if m_z=$-f_y/2$, and θ_{sy}=0 if m_y=$f_z/2$. This reveals that we can exert two transverse forces, on the motion stage, at the symmetric centre of all beams to eliminate the parasitic bending angles. The new action position is

termed as the *centre of stiffness* [18].

3.1.2. DOF analysis of the spatial TBM

When multiplying the normalized compliance matrix (Eq. (8)) by a normalized load vector $[1, 1, 1, 1, 1, 1]^{\mathrm{T}}$, which considers all the load components under the same load magnitude, to generate the normalized displacements, each compliance entry in the compliance matrix can be thought of as the product of the compliance entry times a relevant unit load and represents the contribution of unit load component to the associated displacement. Then we can easily conclude that both the transverse displacements and the torsional angle are DOF whereas the two bending angles and the axial displacement are DOC since these compliance entries associated with the axial displacement and the two bending angles are negligibly smaller than the highlighted diagonal compliance entries associated with the two transverse displacements and the torsional angle.

Let us consider a specific case of spatial TBM whose parameters are: d=10000, r_3=0.6 and L=50mm.

Substituting the above geometrical parameters into Eq. (8), we obtain

$$\mathbf{C}_{\mathrm{p}} = 1\times10^{-3}\begin{bmatrix} 0.0333 & 0 & 0 & 0 & 0 & 0 \\ 0 & \mathbf{[27.824]} & 0 & 0 & 0 & 0.0925 \\ 0 & 0 & \mathbf{[27.824]} & 0 & -0.0925 & 0 \\ 0 & 0 & 0 & \mathbf{[65.700]} & 0 & 0 \\ 0 & 0 & -0.0925 & 0 & 0.1851 & 0 \\ 0 & 0.0925 & 0 & 0 & 0 & 0.1851 \end{bmatrix}. \tag{9}$$

By replacing all the very small entries (approximately in the order of 0.01 of the dominant (highlighted diagonal) compliance entry) in Eq. (9) with 0, Eq. (9) is simplified as

$$\mathbf{C}_{\mathrm{p}} = 1\times10^{-3}\begin{bmatrix} 0 & 0 & 0 & 0 & 0 & 0 \\ 0 & 27.824 & 0 & 0 & 0 & 0 \\ 0 & 0 & 27.824 & 0 & 0 & 0 \\ 0 & 0 & 0 & 65.700 & 0 & 0 \\ 0 & 0 & 0 & 0 & 0 & 0 \\ 0 & 0 & 0 & 0 & 0 & 0 \end{bmatrix}. \tag{10}$$

The above simplified matrix clearly shows that only the two transverse displacements and the torsional angle about the X-axis are the DOF, which provides an easy and direct way to identify DOF/DOC without further complicated derivation/transformation. If there is no normalization applied in the above stiffness modeling (Eqs. (3)–(8)), the compliance matrix of the spatial TBM can be re-expressed as

$$\mathbf{C}_{\text{p-non}} = 1\times10^{-3}\begin{bmatrix} 0.0769 & 0 & 0 & 0 & 0 & 0 \\ 0 & \mathbf{64.1788} & 0 & 0 & 0 & 0.0043 \\ 0 & 0 & \mathbf{64.1788} & 0 & -0.0043 & 0 \\ 0 & 0 & 0 & \mathbf{0.0606} & 0 & 0 \\ 0 & 0 & -0.0043 & 0 & 0.0002 & 0 \\ 0 & 0.0043 & 0 & 0 & 0 & 0.0002 \end{bmatrix}. \tag{11}$$

Different from Eq. (9), the DOF cannot be obtained directly from the non-normalized compliance matrix (Eq. (11)) by comparing the entries due to the different units of compliance entries. This may also mislead some readers to that the torsional angle is the DOC rather than the DOF by direct observation since the compliance entry associated with the torsional angle in Eq. (11) is as small as that associated with the axial displacement.

3.2. Analysis of a spatial double TBM

In compliant mechanism design, one can obtain compliant mechanisms with good performance characteristics such as kinematic-decoupling and reduced primary stiffness, respectively, by symmetrical and serial arranging two modules or more.

A spatial double TBM [21, 22, 27] is shown in Fig. 3. It is composed of two spatial TBMs as two basic building blocks connected in series and has approximately half primary stiffness and double motion range of a single spatial TBM. Here, the global fixed coordinate system, loads and displacements are defined in the same way as the above spatial TBM. The inner and outer pitch radiuses of beams are represented by r_3 and r_3', respectively.

From the nonlinear analysis [27] of the single spatial TBM (Fig. 2), we learn that the axial displacement depends on three components: purely elastic effect only from the axial force, purely kinematic effect, from the three DOF, and elastokinematic effect (the elastokinematic effect is very smaller than purely kinematic effect) of the spatial TBM. However, for the spatial double TBM, the purely kinematic effect upon the axial displacement can be largely eliminated as the transverse forces and torque imposed on the secondary stage produce positive axial displacement to the motion stage, while the transverse forces and torque imposed on the motion stage produce negative axial displacement. In addition, the spatial double TBM can alleviate the load-stiffening effect [5, 27] from the axial force, which makes it suitable for the symmetrical design. The above argument provides a basis for us to 1) use the spatial double TBM as a building block of compliant manipulators [21, 22], and 2) analyze the spatial double TBM using the linear modeling method due to the approximately eliminated nonlinear characteristics such as purely kinematic effect.

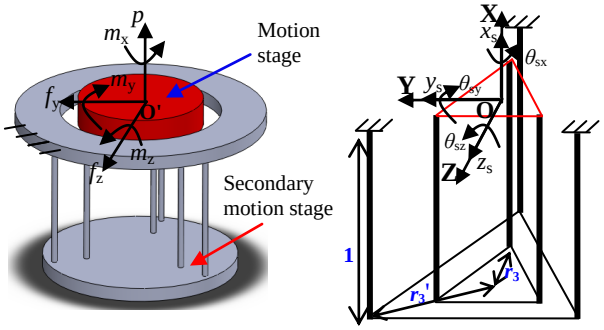

(a) CAD model (b) Schematic model

Fig. 3. A spatial double TBM

The stiffness modeling of the spatial double TBM (Fig. 3) can be derived as the stiffness modeling of compliant serial chains [21, 29].

Since the displacements of the motion stage in the spatial double TBM are caused by both the inner spatial TBM deformation and the outer spatial TBM deformation, we have

$$\mathbf{X}_s = \mathbf{\Delta X}_{s1} + \mathbf{\Delta X}_{s2} \tag{12}$$

where $\mathbf{X}_s = [x_s, y_s, z_s, \theta_{sx}, \theta_{sy}, \theta_{sz}]^T$ is the resulting displacement vector of the motion stage, $\mathbf{\Delta X}_{s1}$ is the displacement vector component of the motion stage resulting from the contribution of the inner spatial TBM deformation alone, $\mathbf{\Delta X}_{s2}$ is the displacement vector component of the motion stage resulting from the contribution of the outer spatial TBM deformation alone.

From Eq. (7), we obtain

$$\mathbf{\Delta X}_{s1} = \mathbf{C}_p\mathbf{F} \tag{13}$$

where $\mathbf{C}_p$, shown in Eq. (8), is the local compliance matrix of the inner spatial TBM. $\mathbf{F} = [p, f_y, f_z, m_x, m_y, m_z]^T$, which is the load vector acting at the motion stage.

Similar to Eq. (3), we further have

$$\mathbf{\Delta X}_{s2} = \mathbf{J}\Delta\mathbf{X}'_{s2} \tag{14}$$

where $\Delta\mathbf{X}'_{s2}$ is the displacement vector of the secondary motion stage and $\mathbf{J}$ is the transformation matrix of the displacements of the secondary motion stage with respect to the global coordinate system O-XYZ. The latter is obtained based on $\mathbf{D}_{pi}$ in Eq. (3) using the relative location (1, 0, 0) of the centre of the motion stage with respect to that of the secondary motion stage.

Based on Eq. (7), we obtain

$$\Delta\mathbf{X}'_{s2} = \mathbf{C}_{p2}\mathbf{F}_2 \tag{15}$$

where $\mathbf{C}_{p2}$, which can be obtained using Eq. (8), is the local compliance matrix of the outer spatial TBM. $\mathbf{F}_2=\mathbf{J}^T\mathbf{F}$, obtained using Eq. (5), is the load vector acting at the secondary motion stage.

Combining Eqs. (12)–(15), the load-displacement equations for the motion stage can be obtained as

$$\mathbf{X}_s = \mathbf{C}_p\mathbf{F} + \mathbf{J}\mathbf{C}_{p2}\mathbf{J}^T\mathbf{F} = (\mathbf{C}_p + \mathbf{J}\mathbf{C}_{p2}\mathbf{J}^T)\mathbf{F} \ . \tag{16}$$

Thus, the compliance matrix for the spatial double TBM can be expressed as

$$\mathbf{C}_s = \mathbf{C}_p + \mathbf{J}\mathbf{C}_{p2}\mathbf{J}^T = \begin{bmatrix} c_{s11} & 0 & 0 & 0 & 0 & 0 \\ 0 & c_{s22} & 0 & 0 & 0 & c_{s26} \\ 0 & 0 & c_{s33} & 0 & c_{s35} & 0 \\ 0 & 0 & 0 & c_{s44} & 0 & 0 \\ 0 & 0 & c_{s53} & 0 & c_{s55} & 0 \\ 0 & c_{s62} & 0 & 0 & 0 & c_{s66} \end{bmatrix} \tag{17}$$

where $\mathbf{C}_{p2}$ and $\mathbf{J}$ are shown in detail as follows:

$$\mathbf{C}_{p2} = \begin{bmatrix} -1 & 0 & 0 & 0 & 0 & 0 \\ 0 & -1 & 0 & 0 & 0 & 0 \\ 0 & 0 & 1 & 0 & 0 & 0 \\ 0 & 0 & 0 & -1 & 0 & 0 \\ 0 & 0 & 0 & 0 & -1 & 0 \\ 0 & 0 & 0 & 0 & 0 & 1 \end{bmatrix} \mathbf{C}_p \begin{bmatrix} -1 & 0 & 0 & 0 & 0 & 0 \\ 0 & -1 & 0 & 0 & 0 & 0 \\ 0 & 0 & 1 & 0 & 0 & 0 \\ 0 & 0 & 0 & -1 & 0 & 0 \\ 0 & 0 & 0 & 0 & -1 & 0 \\ 0 & 0 & 0 & 0 & 0 & 1 \end{bmatrix}^{-1} = \begin{bmatrix} 1/3d & 0 & 0 & 0 & 0 & 0 \\ 0 & \frac{(r_3'^2 d+8)}{36(r_3'^2 d+2)} & 0 & 0 & 0 & \frac{-1}{3(r_3'^2 d+2)} \\ 0 & 0 & \frac{(r_3'^2 d+8)}{36(r_3'^2 d+2)} & 0 & \frac{1}{3(r_3'^2 d+2)} & 0 \\ 0 & 0 & 0 & \frac{625}{9(2500r_3'^2+157)} & 0 & 0 \\ 0 & 0 & \frac{1}{3(r_3'^2 d+2)} & 0 & \frac{2}{3(r_3'^2 d+2)} & 0 \\ 0 & \frac{-1}{3(r_3'^2 d+2)} & 0 & 0 & 0 & \frac{2}{3(r_3'^2 d+2)} \end{bmatrix}, \text{ and}$$

$$\mathbf{J} = \begin{bmatrix} 1 & 0 & 0 & 0 & 0 & 0 \\ 0 & 1 & 0 & 0 & 0 & 1 \\ 0 & 0 & 1 & 0 & -1 & 0 \\ 0 & 0 & 0 & 1 & 0 & 0 \\ 0 & 0 & 0 & 0 & 1 & 0 \\ 0 & 0 & 0 & 0 & 0 & 1 \end{bmatrix}.$$

The entries in $\mathbf{C}_s$ are $c_{s11}=\frac{2}{3d}$, $c_{s22}=\frac{(r_3^2d+8)}{36(r_3^2d+2)}+\frac{(r_3'^2d+8)}{36(r_3'^2d+2)}$, $c_{s26}=\frac{1}{3(r_3^2d+2)}+\frac{1}{3(r_3'^2d+2)}$, $c_{s33}=\frac{(r_3^2d+8)}{36(r_3^2d+2)}+\frac{(r_3'^2d+8)}{36(r_3'^2d+2)}$,

$c_{s35}=\frac{-1}{3(r_3^2d+2)}-\frac{1}{3(r_3'^2d+2)}$, $c_{s44}=\frac{625}{9(2500r_3^2+157)}+\frac{625}{9(2500r_3'^2+157)}$, $c_{s53}=\frac{-1}{3(r_3^2d+2)}-\frac{1}{3(r_3'^2d+2)}$,

$c_{s55}=\frac{2}{3(r_3^2d+2)}+\frac{2}{3(r_3'^2d+2)}$, $c_{s26}=\frac{1}{3(r_3^2d+2)}+\frac{1}{3(r_3'^2d+2)}$, $c_{s66}=\frac{2}{3(r_3^2d+2)}+\frac{2}{3(r_3'^2d+2)}$.

From the above entries of the compliance matrix in Eq. (17), it is shown that under relatively large d (e.g. $d \geq 10000$), the spatial double TBM is still a 3-DOF CPM, but it has half primary stiffness of a spatial TBM. Under the conditions of large enough r_3 and r_3', the spatial double TBM can also be regarded as a 2-DOF compliant module without appreciable torsion. This also applied to the single spatial TBM under large enough pitch circle radius.

4. Spatial tilted multi-beam modules

In this section, we will investigate the modeling of compliance matrices of a spatial tilted TBM and a spatial double tilted TBM and also analyze their DOF.

4.1. Analysis of a spatial tilted TBM

A spatial tilted TBM [31] is shown in Fig. 4. It is composed of a base, three tilted beams and a thin motion stage. The base and motion stage are connected by the tilted three beams. Here, the three beams are uniformly spaced around two circles of radius r_3 and r_3' ($r_3 < r_3'$) on the motion stage and base, respectively, and three central axes of the three beams intersect at one point (named theoretical virtual rotation centre: C).

Based on the type synthesis of CPMs in [16, 28], the CPM in Fig. 4 is a 3-DOF rotational CPM, and all the three rotations are with respect to the theoretical virtual rotation centre C. The external applied loads, displacements of the motion stage and global fixed coordinate system are defined in the same way as in Section 3.1. Three local coordinate systems (O_1-$X_1Y_1Z_1$, O_1-$X_2Y_2Z_2$, and O_3-$X_3Y_3Z_3$) at the tips of the three beams (Figs. 4 (b) and (c)) are further established to facilitate the analysis.

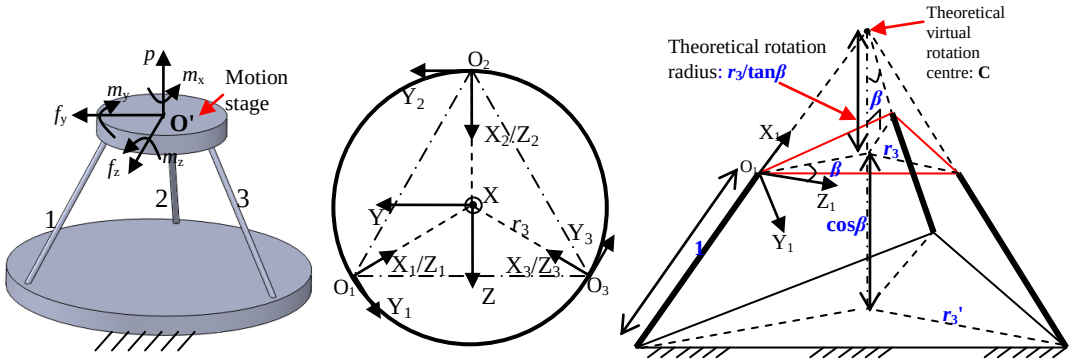

(a) CAD model (b) Top view of motion stage (c) Schematic model

Fig. 4. A spatial tilted TBM

4.1.1. Modeling of the spatial tilted TBM

Similar to the modeling in Section 3.1.1, the geometric compatibility relationships between the displacements of the motion stage centre and the displacements of the i-th tip, with respect to the O_i-$X_iY_iZ_i$ (i=1, 2, 3), can be obtained as

$$\begin{bmatrix} x_i \\ y_i \\ z_i \\ \theta_{ix} \\ \theta_{iy} \\ \theta_{iz} \end{bmatrix} = \mathbf{R}_{Yi}(\beta)\mathbf{R}_X(-\alpha_i)\mathbf{D}_i \begin{bmatrix} x_s \\ y_s \\ z_s \\ \theta_{sx} \\ \theta_{sy} \\ \theta_{sz} \end{bmatrix} \tag{18}$$

$$= \begin{bmatrix} \cos\beta & 0 & \sin\beta & 0 & 0 & 0 \\ 0 & 1 & 0 & 0 & 0 & 0 \\ -\sin\beta & 0 & \cos\beta & 0 & 0 & 0 \\ 0 & 0 & 0 & \cos\beta & 0 & \sin\beta \\ 0 & 0 & 0 & 0 & 1 & 0 \\ 0 & 0 & 0 & -\sin\beta & 0 & \cos\beta \end{bmatrix} \begin{bmatrix} 1 & 0 & 0 & 0 & 0 & 0 \\ 0 & \cos\alpha_i & \sin\alpha_i & 0 & 0 & 0 \\ 0 & -\sin\alpha_i & \cos\alpha_i & 0 & 0 & 0 \\ 0 & 0 & 0 & 1 & 0 & 0 \\ 0 & 0 & 0 & 0 & \cos\alpha_i & \sin\alpha_i \\ 0 & 0 & 0 & 0 & -\sin\alpha_i & \cos\alpha_i \end{bmatrix} \begin{bmatrix} 1 & 0 & 0 & 0 & z_i' & -y_i' \\ 0 & 1 & 0 & -z_i' & 0 & x_i' \\ 0 & 0 & 1 & y_i' & -x_i' & 0 \\ 0 & 0 & 0 & 1 & 0 & 0 \\ 0 & 0 & 0 & 0 & 1 & 0 \\ 0 & 0 & 0 & 0 & 0 & 1 \end{bmatrix} \begin{bmatrix} x_s \\ y_s \\ z_s \\ \theta_{sx} \\ \theta_{sy} \\ \theta_{sz} \end{bmatrix}$$

where x_i, y_i, z_i, θ_{ix}, θ_{iy} and θ_{iz} (i=1, 2, 3) are the displacements of the i-th tip with respect to O_i-$X_iY_iZ_i$. x_i', y_i' and z_i' are the relative location parameters of the i-th tip with respect to the centre, O', of the motions stage. $\alpha_1=2\pi/3$, $\alpha_2=0$, $\alpha_3=-2\pi/3$.

Then, the load-displacement equations for the i-th tip with respect to O_i-$X_iY_iZ_i$ is

$$\begin{bmatrix} p_i \\ f_{iy} \\ f_{iz} \\ m_{ix} \\ m_{iy} \\ m_{iz} \end{bmatrix} = \mathbf{K}_i \begin{bmatrix} x_i \\ y_i \\ z_i \\ \theta_{ix} \\ \theta_{iy} \\ \theta_{iz} \end{bmatrix} = \begin{bmatrix} d & 0 & 0 & 0 & 0 & 0 \\ 0 & a & 0 & 0 & 0 & c \\ 0 & 0 & a & 0 & -c & 0 \\ 0 & 0 & 0 & \delta & 0 & 0 \\ 0 & 0 & -c & 0 & b & 0 \\ 0 & c & 0 & 0 & 0 & b \end{bmatrix} \begin{bmatrix} x_i \\ y_i \\ z_i \\ \theta_{ix} \\ \theta_{iy} \\ \theta_{iz} \end{bmatrix} \tag{19}$$

where p_i, f_{iy}, f_{iz}, m_{ix}, m_{iy} and m_{iz} (i=1, 2, 3), denote the loads acting at the i-th tip with respect to O_i-$X_iY_iZ_i$.

Further, the load-equilibrium conditions for the motion stage can be obtained as

$$\begin{bmatrix} p \\ f_y \\ f_z \\ m_x \\ m_y \\ m_z \end{bmatrix} = \sum_{i=1}^{n=3} \mathbf{D}_i^{\mathrm{T}} \mathbf{R}_{\mathrm{X}}^{\mathrm{T}}(-\alpha_i) \mathbf{R}_{\mathrm{Y}i}^{\mathrm{T}}(\beta) \begin{bmatrix} p_i \\ f_{iy} \\ f_{iz} \\ m_{ix} \\ m_{iy} \\ m_{iz} \end{bmatrix} \tag{20}$$

where $\mathbf{D}_i$, $\mathbf{R}_X(-\alpha_i)$ and $\mathbf{R}_{Yi}(\beta)$ (i=1, 2, 3) are those matrices shown in Eq. (18).

Combining Eqs. (18)–(20), we obtain the load-displacement equations for the motion stage as:

$$\mathbf{X}_{\mathrm{s}} = \mathbf{K}_{\mathrm{p1}}^{-1}\mathbf{F} = \mathbf{C}_{\mathrm{p1}}\mathbf{F} \tag{21}$$

where $\mathbf{X}_{\mathrm{s}} = [x_{\mathrm{s}}, y_{\mathrm{s}}, z_{\mathrm{s}}, \theta_{\mathrm{sx}}, \theta_{\mathrm{sy}}, \theta_{\mathrm{sz}}]^{\mathrm{T}}$ and $\mathbf{F} = [p, f_{\mathrm{y}}, f_{\mathrm{z}}, m_{\mathrm{x}}, m_{\mathrm{y}}, m_{\mathrm{z}}]^{\mathrm{T}}$. $\mathbf{K}_{\mathrm{p1}} = \sum_{i=1}^{3} \mathbf{D}_i^{\mathrm{T}} \mathbf{R}_{\mathrm{X}}^{\mathrm{T}}(-\alpha_i) \mathbf{R}_{\mathrm{Y}i}^{\mathrm{T}}(\beta) \mathbf{K}_i \mathbf{R}_{\mathrm{Y}i}(\beta) \mathbf{R}_{\mathrm{X}}(-\alpha_i) \mathbf{D}_i$, which is the stiffness matrix of the spatial tilted TBM. $\mathbf{C}_{\mathrm{p1}} = \mathbf{K}_{\mathrm{p1}}^{-1}$, which is its compliance matrix accordingly.

4.1.2. DOF analysis of the spatial tilted TBM

Consider the spatial tilted TBM shown in Fig. 4, let $\beta=\pi/4$, L=50 (mm), r_3=0.6 and d=10000 (x_1'=0, $y_1'=r_3\sin(\pi/3)$, $z_1'=r_3\cos(\pi/3)$ for tip 1, x_2'=0, y_2'=0, $z_2'=-r_3$ for tip 2, x_3'=0, $y_3'=-r_3\sin(\pi/3)$, $z_3'=r_3\cos(\pi/3)$ for tip 3). The material for this module is the same aluminium alloy as detailed in Section 3.1.1. From Eqs. (18)–(21), we obtain the compliance matrix

$$\mathbf{C}_{\mathrm{p1}} = 1\times10^{-3}\begin{bmatrix} 0.0666 & 0 & 0 & 0 & 0 & 0 \\ 0 & \mathbf{6.983} & 0 & 0 & 0 & \mathbf{-11.504} \\ 0 & 0 & \mathbf{6.983} & 0 & \mathbf{11.504} & 0 \\ 0 & 0 & 0 & \mathbf{28.277} & 0 & 0 \\ 0 & 0 & \mathbf{11.504} & 0 & \mathbf{19.320} & 0 \\ 0 & \mathbf{-11.504} & 0 & 0 & 0 & \mathbf{19.320} \end{bmatrix}. \tag{22}$$

If ignoring some insignificant entries in $\mathbf{C}_{\mathbf{p1}}$, Eq. (22) can be simplified as

$$\mathbf{C}_{\mathrm{p1}} = 1\times10^{-3}\begin{bmatrix} 0 & 0 & 0 & 0 & 0 & 0 \\ 0 & 6.983 & 0 & 0 & 0 & -11.504 \\ 0 & 0 & 6.983 & 0 & 11.504 & 0 \\ 0 & 0 & 0 & 28.277 & 0 & 0 \\ 0 & 0 & 11.504 & 0 & 19.320 & 0 \\ 0 & -11.504 & 0 & 0 & 0 & 19.320 \end{bmatrix}. \tag{23}$$

From Eq. (23), it is observed that

$$y_{\mathrm{s}} \approx -(6.893/11.504)\theta_{\mathrm{sz}} \approx -(11.504/19.320)\theta_{\mathrm{sz}} \approx -[0.6/\tan(\beta)]\theta_{\mathrm{sz}},$$
$$z_{\mathrm{s}} \approx (6.893/11.504)\theta_{\mathrm{sy}} \approx (11.504/19.320)\theta_{\mathrm{sy}} \approx [0.6/\tan(\beta)]\theta_{\mathrm{sy}}.$$

i.e. two transverse displacements are not independent of the rotations. Analogous to the DOF analysis in Section 3.1.2, it is clear that the spatial tilted TBM has three DOF, which can be represented by the three rotational angles as discussed below. Here, the negligible difference such as $|6.983/11.504-0.6|=0.007$ or $|11.504/19.320-0.6|=0.0046$ is the well-known centre-drift [32]. Equations (22) or (23) also shows that $y_{\mathrm{s}}=\theta_{\mathrm{sz}}\approx0$ if $m_{\mathrm{z}}=0.6f_{\mathrm{y}}$, and $z_{\mathrm{s}}=\theta_{\mathrm{sy}}\approx0$ if $m_{\mathrm{y}}=-0.6f_{\mathrm{z}}$. This reveals that two transverse forces, exerted on the motion stage at the position of the theoretical virtual rotation centre, can not cause any motion.

The compliance matrix $\mathbf{C}_{\mathrm{p1}}$ can be regarded to be composed of six screws [13] in order to reveal the motion characteristics more effectively. Equation (22) can be rewritten as

$$\mathbf{C}_{\mathrm{p1}} = [\mathbf{s}_1, \mathbf{s}_2, \mathbf{s}_3, \mathbf{s}_4, \mathbf{s}_5, \mathbf{s}_6] \approx \begin{bmatrix} \mathbf{0} & \mathbf{v}_2 & \mathbf{v}_3 & \mathbf{v}_4 & \mathbf{v}_5 & \mathbf{v}_6 \\ \mathbf{0} & \mathbf{w}_2 & \mathbf{w}_3 & \mathbf{w}_4 & \mathbf{w}_5 & \mathbf{w}_6 \end{bmatrix} \tag{24}$$

where

0 denotes a 3 by 1 zero vector,

$\mathbf{s}_i$ (i=2, 3, …, 6) denotes the screws,

$\mathbf{w}_2$ denotes the rotation vector along the −Z-axis,

$\mathbf{w}_3$ denotes the rotation vector along the Y-axis,

$\mathbf{w}_4$ denotes the rotation vector along the X-axis,
$\mathbf{w}_5$ denotes the rotation vector along the Y-axis ,
$\mathbf{w}_6$ denotes the rotation vector along the Z-axis,
$\boldsymbol{v}_i$ (i=1, 2,…, 6) denotes the translational displacement vector,

$$\mathbf{v}_2 = \mathbf{r}_2 \times \mathbf{w}_2 + p_2 \mathbf{w}_2 ,$$

$$\mathbf{v}_3 = \mathbf{r}_3 \times \mathbf{w}_3 + p_3 \mathbf{w}_3 ,$$

$$\mathbf{v}_4 = \mathbf{r}_4 \times \mathbf{w}_4 + p_4 \mathbf{w}_4 ,$$

$$\mathbf{v}_5 = \mathbf{r}_5 \times \mathbf{w}_5 + p_5 \mathbf{w}_5 ,$$

$$\mathbf{v}_6 = \mathbf{r}_6 \times \mathbf{w}_6 + p_6 \mathbf{w}_6 ,$$

p_i (i=1, 2,…, 6) denotes the pitch of the i-th screw,
$\mathbf{r}_i$ (i=1, 2,…, 6) denotes the position vector of any point on the corresponding screw axis with respect to the fixed coordinate system.
All the pitches can be obtained as

$$p_2 = \frac{\mathbf{v}_2 \cdot \mathbf{w}_2}{\mathbf{w}_2 \cdot \mathbf{w}_2} = 0 ;\ p_3 = \frac{\mathbf{v}_3 \cdot \mathbf{w}_3}{\mathbf{w}_3 \cdot \mathbf{w}_3} = 0 ;\ p_4 = \frac{\mathbf{v}_4 \cdot \mathbf{w}_4}{\mathbf{w}_4 \cdot \mathbf{w}_4} = 0 ;\ p_5 = \frac{\mathbf{v}_5 \cdot \mathbf{w}_5}{\mathbf{w}_5 \cdot \mathbf{w}_5} = 0 ;\ \ p_6 = \frac{\mathbf{v}_6 \cdot \mathbf{w}_6}{\mathbf{w}_6 \cdot \mathbf{w}_6} = 0 . \tag{25}$$

Each rotation radius (the magnitude of the minimal position vector) of the centre of the motion stage with respect to the relevant real screw axis (Fig. 5) can be further obtained as

$$\underline{r}_2 = \frac{|\mathbf{v}_2|}{|\mathbf{w}_2|} = 0.607 \approx 0.6; \underline{r}_3 = \frac{|\mathbf{v}_3|}{|\mathbf{w}_3|} = 0.607 \approx 0.6; \underline{r}_4 = \frac{|\mathbf{v}_4|}{|\mathbf{w}_4|} = 0; \underline{r}_5 = \frac{|\mathbf{v}_5|}{|\mathbf{w}_5|} = 0.5954 \approx 0.6; \underline{r}_6 = \frac{|\mathbf{v}_6|}{|\mathbf{w}_6|} = 0.5954 \approx 0.6 \ . \tag{26}$$

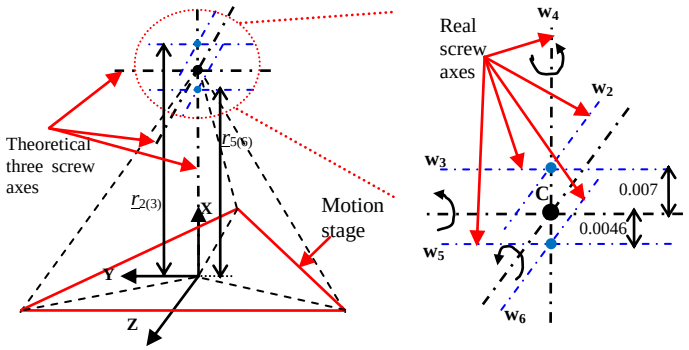

Fig. 5. Illustration for real screw axes and theoretical screw axes

Figure 5 shows that the real screw axis $\mathbf{w}_3$ ($\mathbf{w}_5$) is very close to the corresponding theoretical screw axis which goes through the point C and is parallel to the Y-axis. The distance between the two axes is 0.007(or 0.0046), negligible compared with the theoretical rotation radius of 0.6. Therefore, the real screw axis $\mathbf{w}_3$ ($\mathbf{w}_5$) can be thought of as overlapping with the theoretical axis parallel to the Y-axis. Similarly, the real screw axis $\mathbf{w}_2$ ($\mathbf{w}_6$) can be thought of as overlapping with the theoretical axis parallel to the Z-axis. These approximations reveal that the spatial tilted TBM is a 3-DOF rotational CPM.

The above analysis shows that only the independent *pure rotations* about the virtual rotation centre are the DOF.

If there is no normalization applied in the above stiffness modeling (Eqs. (18)–(21)), the compliance matrix of the spatial tilted TBM can be re-expressed as follows:

$$\mathbf{C}_{\text{p1-non}} = 1\times10^{-3}\begin{bmatrix} 0.1536 & 0 & 0 & 0 & 0 & 0 \\ 0 & \mathbf{16.107} & 0 & 0 & 0 & \mathbf{-0.531} \\ 0 & 0 & \mathbf{16.107} & 0 & \mathbf{0.531} & 0 \\ 0 & 0 & 0 & \mathbf{0.0261} & 0 & 0 \\ 0 & 0 & \mathbf{0.531} & 0 & \mathbf{0.0178} & 0 \\ 0 & \mathbf{-0.531} & 0 & 0 & 0 & \mathbf{0.0178} \end{bmatrix} . \tag{27}$$

This non-normalized compliance matrix (Eq. (27)) has no such characteristics as shown in Eq. (22), and may mislead to that x_s is the DOF, and θ_{sx} is the DOC for some readers by direct observation since the compliance entry associated with the translational displacement along the X-axis (x_s) is larger than that associated with the rotation about the X-axis (θ_{sx}).

An inverted spatial tilted TBM is shown in Fig. 6. The coordinate system, loads and displacements are all defined in the same way as in Fig. 4. Similarly, the compliance matrix for the inverted spatial tilted TBM is derived as

$$\mathbf{C}_{\text{p2}} = [\sum_{i=1}^{3} \mathbf{D}_i^{\text{T}} \mathbf{R}_{\text{X}}^{\text{T}}(-\alpha_i) \mathbf{R}_{\text{Y}i}^{\text{T}}(-\beta) \mathbf{K}_i \mathbf{R}_{\text{Y}i}(-\beta) \mathbf{R}_{\text{X}}(-\alpha_i) \mathbf{D}_i]^{-1} \ . \tag{28}$$

Let L=50 (mm), d=10000, β=π/4, r_3=0.6 and r_3'=r_3+sinβ=1.307 (x_1'=0, y_1'=r_3'sin(π/3), z_1'=r_3'cos(π/3) for the tip 1, x_2'=0, y_2'=0, z_2'=$-r_3$ 'for the tip 2, x_3'=0, y_3'=$-r_3'$sin(π/3), z_3'=r_3'cos(π/3) for the tip 3), we have

$$\mathbf{C}_{p2}=1\times10^{-3}\begin{bmatrix}0.0666 & 0 & 0 & 0 & 0 & 0\\ 0 & 32.912 & 0 & 0 & 0 & 25.166\\ 0 & 0 & 32.912 & 0 & -25.166 & 0\\ 0 & 0 & 0 & 28.277 & 0 & 0\\ 0 & 0 & -25.166 & 0 & 19.320 & 0\\ 0 & 25.166 & 0 & 0 & 0 & 19.320\end{bmatrix}. \tag{29}$$

From Eq. (29), it is observed that

$$y_s\approx[0.6/\tan(\beta)+\cos(\beta)]\,\theta_{sz}=1.307\theta_{sz},\ z_s\approx-[0.6/\tan(\beta)+\cos(\beta)]\,\theta_{sy}=-1.307\theta_{sy}.$$

This reveals that the motion stage of this inverted spatial tilted TBM can produce large translation than the original one under same rotation since the theoretical rotational radius, 1.307, of the inverted module is larger than that, 0.6, of the original module.

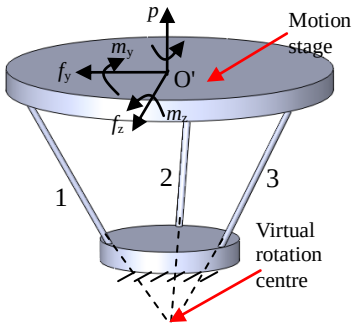

Fig. 6. An inverted spatial tilted TBM

4.2. Analysis of a spatial double tilted TBM

Analogous to the generation of the spatial double TBM (Fig. 3), we can combine two spatial tilted TBMs as two basic building blocks in series to obtain a spatial double tilted TBM shown in Fig. 7. This mechanism has approximately double motion stage and half stiffness of a single spatial tilted TBM as detailed below.

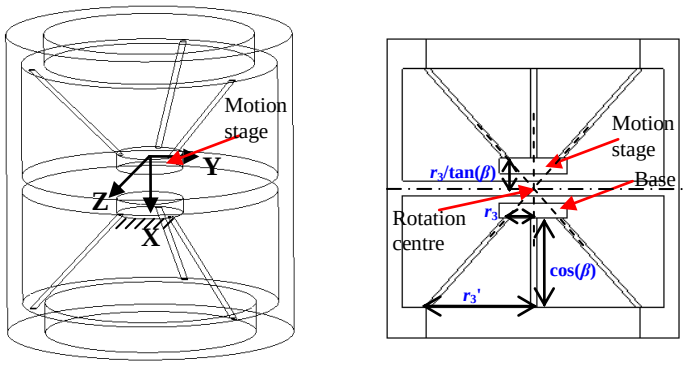

(a) 3-D view of CAD model (b) Front view of CAD model

Fig. 7. A spatial double tilted TBM

Based on Eqs. (17), (21) and (28), we obtain the compliance matrix for the spatial double tilted TBM:

$$\mathbf{C}_s=\mathbf{C}_{p1}+\mathbf{J}\mathbf{C}_{p2}\mathbf{J}^{\mathrm{T}}. \tag{30}$$

where $\mathbf{C}_{p1}$ and $\mathbf{C}_{p2}$ are the compliance matrices shown in Eqs. (21) and (28), respectively, and

$$\mathbf{J}=\begin{bmatrix}1 & 0 & 0 & 0 & 0 & 0\\ 0 & 1 & 0 & 0 & 0 & -2r_3/\tan\beta-\cos\beta\\ 0 & 0 & 1 & 0 & 2r_3/\tan\beta+\cos\beta & 0\\ 0 & 0 & 0 & 1 & 0 & 0\\ 0 & 0 & 0 & 0 & 1 & 0\\ 0 & 0 & 0 & 0 & 0 & 1\end{bmatrix}.$$

Substituting all the geometric parameters into Eq. (30), we obtain

$$\mathbf{C}_S = 1\times10^{-3}\begin{bmatrix} 0.1332 & 0 & 0 & 0 & 0 & 0 \\ 0 & 14.1744 & 0 & 0 & 0 & -23.1833 \\ 0 & 0 & 14.1744 & 0 & 23.1833 & 0 \\ 0 & 0 & 0 & 56.5540 & 0 & 0 \\ 0 & 0 & 23.1833 & 0 & 38.6400 & 0 \\ 0 & -23.1833 & 0 & 0 & 0 & 38.6400 \end{bmatrix}. \quad (31)$$

Compared with Eq. (22), Eq. (31) shows that the spatial double tilted TBM is also a 3-DOF purely rotational CPM, but has approximately half rotational stiffness of a spatial tilted TBM (for example, element (6, 2) of $\mathbf{C}_{p1}$ (Eq. (22)), is approximately half that of $\mathbf{C}_S$ (Eq. (31))).

The normalization-based strategy can also be used to deal with the DOF identification of other spatial multi-beam modules such as the spatial double tilted four-beam module shown in Fig. 8, and spatial compliant modules composed of sheets such as those discussed in Appendices A and B as well as the error analysis of spatial multi-beam modules with beams of compatible length (Appendix C).

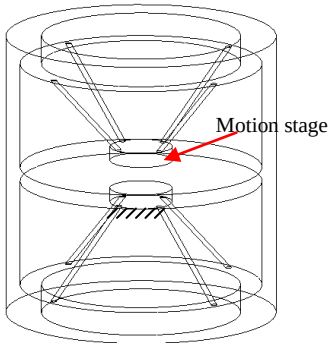

Fig. 8. A spatial double tilted four-beam module

5. Conclusions

This paper has analyzed the mobility of several spatial CPMs, especially spatial multi-beam modules, using a normalization-based approach. The DOF/DOC can be identified more easily from the compliance matrices using the proposed approach than the approach without normalization.

It is noted that the rotational angles and translational displacements (or the forces and moments) have been compared reasonably through the use of a normalization-based approach to deal with the issue of dimension inconsistency, and the normalized load vector with load components under the same load magnitude has also been adopted to ensure the loading magnitude consistency.

The proposed approach may provide an easy way to identify the DOF/DOC of a class of spatial CPMs directly from the normalized compliance matrices without complicated derivation/transformation. This determination of DOF of other classes of compliant mechanisms is still an open issue that deserves further investigation.

Acknowledgement

The authors would like to acknowledge the anonymous reviewers for their invaluable comments on improving the original version of this paper.

Appendices

In the appendices, we will discuss the normalization method for spatial compliant modules composed of identical and uniform sheets (usually long-side length/ short-side length of a rectangular cross-section>10), and also illustrate how to apply the normalization-based approach to the error analysis of spatial multi-beam modules with beams of compatible length. Here, the global coordinate system, loads and displacements are defined in the similar way as previously mentioned.

A. Parallelogram module with two sheets

For the normalization of spatial compliant modules composed of identical and uniform sheets (i.e. spatial compliant multi-sheet modules), all translational displacements and length parameters are divided by the sheet length L, forces by $E'I/L^2$, and moments by $E'I/L$. Here, E' $[E/(1-\nu^2)]$ and I denote, respectively, the plate modulus and the second moment of the area of a rectangular cross-section of the sheet about the central axis parallel to its long side.

We first analyze the common-used parallelogram module (Fig. A.1). From the books on mechanics of materials (see [33] for example), the torsional stiffness for a typical sheet is $G(uL)(tL)^3/(3L)$. Similar to the formulation of Eq. (2), the stiffness matrix for each sheet under the coordinate system O-XYZ can be derived as

$$\mathbf{K}_{1(2)} = \begin{bmatrix} 12(1-v^2)/t^2 & 0 & 0 & 0 & 0 & 0 \\ 0 & 12 & 0 & 0 & 0 & -6 \\ 0 & 0 & 12(u/t)^2(1-v^2) & 0 & 6(u/t)^2(1-v^2) & 0 \\ 0 & 0 & 0 & 2(1-v) & 0 & 0 \\ 0 & 0 & 6(u/t)^2(1-v^2) & 0 & 4(u/t)^2(1-v^2) & 0 \\ 0 & -6 & 0 & 0 & 0 & 4 \end{bmatrix} \quad \text{(A.1)}$$

where u and t are the normalized geometrical parameters of a sheet as shown in Fig. A.1(b). It is noted that there is plane stress in the XZ plane, and there is plane strain in the XY plane.

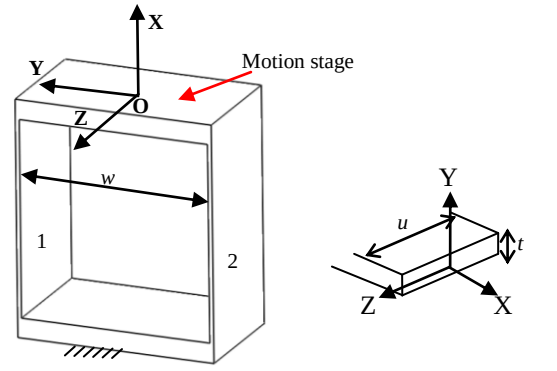

(a) 3-D view of CAD model (b) Dimension of a sheet

Fig. A.1. Parallelogram module with two sheets

Then, the transformation matrices of the displacements of the motion stage are represented as

$$\mathbf{D}_{p1} = \begin{bmatrix} 1 & 0 & 0 & 0 & 0 & -w/2 \\ 0 & 1 & 0 & 0 & 0 & 0 \\ 0 & 0 & 1 & w/2 & 0 & 0 \\ 0 & 0 & 0 & 1 & 0 & 0 \\ 0 & 0 & 0 & 0 & 1 & 0 \\ 0 & 0 & 0 & 0 & 0 & 1 \end{bmatrix} \text{ and } \mathbf{D}_{p2} = \begin{bmatrix} 1 & 0 & 0 & 0 & 0 & w/2 \\ 0 & 1 & 0 & 0 & 0 & 0 \\ 0 & 0 & 1 & -w/2 & 0 & 0 \\ 0 & 0 & 0 & 1 & 0 & 0 \\ 0 & 0 & 0 & 0 & 1 & 0 \\ 0 & 0 & 0 & 0 & 0 & 1 \end{bmatrix} \quad \text{(A.2)}$$

where w is the normalized spacing parameter as shown in Fig. A.1(a).

Therefore, the compliance matrix for the motion stage centre is obtained using Eqs. (A.1) and (A.2) as follows.

$$\mathbf{C}_p = (\mathbf{D}_{p1}^T \mathbf{K}_1 \mathbf{D}_{p1} + \mathbf{D}_{p2}^T \mathbf{K}_2 \mathbf{D}_{p2})^{-1} \quad . \quad \text{(A.3)}$$

As an example, let L=50 (mm), W=50 (mm), T=1 (mm), U=20 (mm) and v=0.3. The substitution of all the normalized values into Eq. (A.3) yields

$$\mathbf{C}_p = 1\times10^{-3} \begin{bmatrix} 0.0183 & 0 & 0 & 0 & 0 & 0 \\ 0 & \mathbf{41.6850} & 0 & 0 & 0 & 0.0366 \\ 0 & 0 & 0.4579 & 0 & -0.6868 & 0 \\ 0 & 0 & 0 & 0.4573 & 0 & 0 \\ 0 & 0 & -0.6868 & 0 & 1.3736 & 0 \\ 0 & 0.03636 & 0 & 0 & 0 & 0.0732 \end{bmatrix} . \quad \text{(A.4)}$$

Equation (A.4) shows that the translation along the Y-axis is the only DOF since the highlighted compliance element, (2, 2), associated with the transverse displacement along the Y-axis is much larger than the other elements, which complies with the qualitative analysis.

B. Four-Sheet Rotational Module

A four-sheet module is shown in Fig. B.1. This module, proposed in [17] as a rotational joint, is composed of four non-tilted sheets in parallel. Here, the neutral surface of each sheet, associated with the bending about the central axis parallel to the long side of its cross-section, passes the central axis of this module.

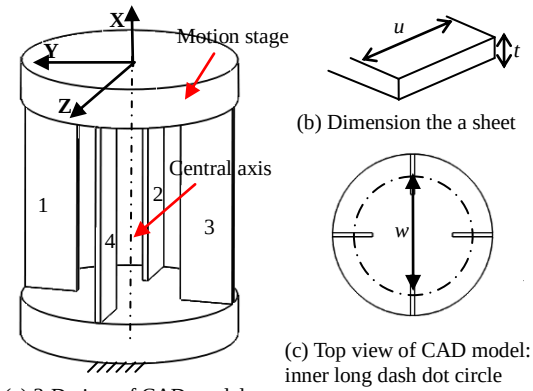

(a) 3-D view of CAD model

(b) Dimension the a sheet

(c) Top view of CAD model: inner long dash dot circle intersecting with the centres

Fig. B.1. Four-sheet rotational module

Analogous to the derivation of Eq. (2), the stiffness matrices for the sheets under the coordinate system O-XYZ can be derived as

$$\mathbf{K}_{1(3)} = \begin{bmatrix} 12(1-v^2)/t^2 & 0 & 0 & 0 & 0 & 0 \\ 0 & 12(u/t)^2(1-v^2) & 0 & 0 & 0 & -6(u/t)^2(1-v^2) \\ 0 & 0 & 12 & 0 & 6 & 0 \\ 0 & 0 & 0 & 2(1-v) & 0 & 0 \\ 0 & 0 & 6 & 0 & 4 & 0 \\ 0 & -6(u/t)^2(1-v^2) & 0 & 0 & 0 & 4(u/t)^2(1-v^2) \end{bmatrix},$$

$$\mathbf{K}_{2(4)} = \begin{bmatrix} 12(1-v^2)/t^2 & 0 & 0 & 0 & 0 & 0 \\ 0 & 12 & 0 & 0 & 0 & -6 \\ 0 & 0 & 12(u/t)^2(1-v^2) & 0 & 6(u/t)^2(1-v^2) & 0 \\ 0 & 0 & 0 & 2(1-v) & 0 & 0 \\ 0 & 0 & 6(u/t)^2(1-v^2) & 0 & 4(u/t)^2(1-v^2) & 0 \\ 0 & -6 & 0 & 0 & 0 & 4 \end{bmatrix} \quad \text{(B.1)}$$

where u and t are the normalized parameters of a sheet as shown in Fig. B.1(b).

The transformation matrices of the displacements of the motion stage are represented as

$$\mathbf{D}_{p1} = \begin{bmatrix} 1 & 0 & 0 & 0 & 0 & -w/2 \\ 0 & 1 & 0 & 0 & 0 & 0 \\ 0 & 0 & 1 & w/2 & 0 & 0 \\ 0 & 0 & 0 & 1 & 0 & 0 \\ 0 & 0 & 0 & 0 & 1 & 0 \\ 0 & 0 & 0 & 0 & 0 & 1 \end{bmatrix}; \mathbf{D}_{p2} = \begin{bmatrix} 1 & 0 & 0 & 0 & -w/2 & 0 \\ 0 & 1 & 0 & w/2 & 0 & 0 \\ 0 & 0 & 1 & 0 & 0 & 0 \\ 0 & 0 & 0 & 1 & 0 & 0 \\ 0 & 0 & 0 & 0 & 1 & 0 \\ 0 & 0 & 0 & 0 & 0 & 1 \end{bmatrix}; \mathbf{D}_{p3} = \begin{bmatrix} 1 & 0 & 0 & 0 & 0 & w/2 \\ 0 & 1 & 0 & 0 & 0 & 0 \\ 0 & 0 & 1 & -w/2 & 0 & 0 \\ 0 & 0 & 0 & 1 & 0 & 0 \\ 0 & 0 & 0 & 0 & 1 & 0 \\ 0 & 0 & 0 & 0 & 0 & 1 \end{bmatrix}; \mathbf{D}_{p4} = \begin{bmatrix} 1 & 0 & 0 & 0 & w/2 & 0 \\ 0 & 1 & 0 & -w/2 & 0 & 0 \\ 0 & 0 & 1 & 0 & 0 & 0 \\ 0 & 0 & 0 & 1 & 0 & 0 \\ 0 & 0 & 0 & 0 & 1 & 0 \\ 0 & 0 & 0 & 0 & 0 & 1 \end{bmatrix} \quad \text{(B.2)}$$

where w is the normalized spacing parameter as shown in Fig. B.1(c).

Then, the compliance matrix for the motion stage centre is obtained using Eqs. (B.1) and (B.2) as follows.

$$\mathbf{C}_p = (\mathbf{D}_{p1}^T\mathbf{K}_1\mathbf{D}_{p1} + \mathbf{D}_{p2}^T\mathbf{K}_2\mathbf{D}_{p2} + \mathbf{D}_{p3}^T\mathbf{K}_3\mathbf{D}_{p3} + \mathbf{D}_{p4}^T\mathbf{K}_4\mathbf{D}_{p4})^{-1}. \quad \text{(B.3)}$$

As an example, let L=50 (mm), W=50 (mm), T=1 (mm), U=20 (mm) and v=0.3. Substituting all the normalized values into Eq. (B.3), we have

$$\mathbf{C}_p = 1\times10^{-3}\begin{bmatrix} 0.0092 & 0 & 0 & 0 & 0 & 0 \\ 0 & 0.1315 & 0 & 0 & 0 & 0.0348 \\ 0 & 0 & 0.1315 & 0 & -0.0348 & 0 \\ 0 & 0 & 0 & \mathbf{56.8182} & 0 & 0 \\ 0 & 0 & -0.0348 & 0 & 0.0695 & 0 \\ 0 & 0.0348 & 0 & 0 & 0 & 0.0695 \end{bmatrix}. \quad \text{(B4)}$$

Equation (B.4) shows that the torsion about the X-axis is the only DOF since the highlighted compliance element, (4, 4) associated with the torsion about the X-axis is much larger than the other elements, which complies with the qualitative analysis.

Similar to the design in Section 3.2, we can also obtain an improved rotational joint: double four-sheet rotational joint as shown in Fig. B.2. It doubles the rotational range without rotation centre-drift, and alleviates the parasitic axial translational displacement along the X-axis.

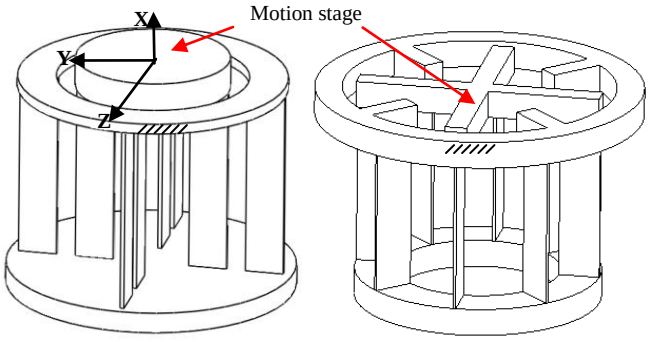

a) Type 1 b) Type 2

Fig. B.2. Double four-sheet rotational modules: a) eight sheets distributed along two circles (largely eliminating the parasitic axial translation accompanying the primary torsion), and b) eight sheets distributed along one circle (completely eliminating the parasitic axial translation accompanying the primary torsion)

C. Spatial TBM error analysis

In this section, the error analysis of a spatial TBM will be dealt with to analyze the affect of the beam length error on the normalized compliance matrix for the DOF identification. In turn, the derived compliance matrix can be used to diagnose the length error.

Here, we only discuss the case in which two beams (Beams 1 and 3) are of length L_1, and one beam (beam 2) is of length L_2 (Fig. C.1).

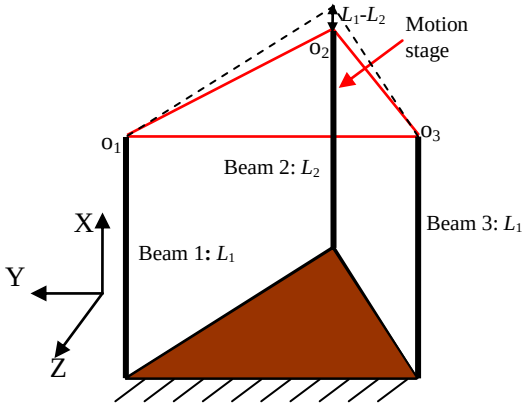

Fig. C.1. Variation of the spatial TBM

Let L_1 be the characteristic length for normalization. Then the normalized stiffness matrices for Beam 1 or Beam 3 remain unchanged as **K** shown in Eq. (2), while that for Beam 2 is derived based on the normalization method as follows:

$$\mathbf{K}_2 = \begin{bmatrix} (L_1/L_2)d & 0 & 0 & 0 & 0 & 0 \\ 0 & (L_1/L_2)^3 a & 0 & 0 & 0 & (L_1/L_2)^2 c \\ 0 & 0 & (L_1/L_2)^3 a & 0 & -(L_1/L_2)^2 c & 0 \\ 0 & 0 & 0 & (L_1/L_2)\delta & 0 & 0 \\ 0 & 0 & -(L_1/L_2)^2 c & 0 & (L_1/L_2)b & 0 \\ 0 & (L_1/L_2)^2 c & 0 & 0 & 0 & (L_1/L_2)b \end{bmatrix}. \tag{C.1}$$

where d=16/$(D/L_1)^2$ for round beams or d=12/$(T/L_1)^2$ for square beams.

Form Eq. (C.1), it can be observed that if L_2 is significantly smaller than L_1, compared with the more compliant Beams 1 and 3, Beam 2 from a 5-DOF compliant mechanism excluding the axial displacement degenerates to

a) a 3-DOF spherical joint due to the fact that all the stiffness entries associated with the two transverse displacements (elements (2,2), (2,6), (3,3), and (3,5)) are very large resulting from the existence of high-order terms of L_1/L_2, or

b) even a DOC if all the stiffness entries associated with the three rotational angles are also very large under the conditions that the first-order terms of L_1/L_2 (elements (4,4), (5,5) and (6,6)) are large enough.

Let Δ=1−L_2/L_1 be the small error, we have

$$\frac{L_1}{L_2} = \frac{1}{1-\Delta} = \frac{1+\Delta}{1-\Delta^2} \approx 1+\Delta\,. \tag{C.2}$$

Further, based on Taylor series expansion, we obtain

$$(1\pm\Delta)^n \approx 1\pm n\Delta\,. \tag{C.3}$$

Therefore, we can re-write the above stiffness matrix (Eq. (C.1)) as

$$\mathbf{K}_2 = \begin{bmatrix} (1+\Delta)d & 0 & 0 & 0 & 0 & 0 \\ 0 & (1+3\Delta)a & 0 & 0 & 0 & (1+2\Delta)c \\ 0 & 0 & (1+3\Delta)a & 0 & -(1+2\Delta)c & 0 \\ 0 & 0 & 0 & (1+\Delta)\delta & 0 & 0 \\ 0 & 0 & -(1+2\Delta)c & 0 & (1+\Delta)b & 0 \\ 0 & (1+2\Delta)c & 0 & 0 & 0 & (1+\Delta)b \end{bmatrix}. \quad \text{(C.4)}$$

Using the stiffness method in Section 3.1.1 to obtain the normalized compliance matrix for the spatial TBM with length error, and substituting the same known conditions for Eq. (9) and Δ=0.05 into the result, we have

$$\mathbf{C}_{\text{cpm-error}} = 1\times10^{-3}\begin{bmatrix} 0.0328 & 0 & -0.0009 & 0 & 0.0018 & 0 \\ 0 & \mathbf{[25.5513]} & 0 & -1.8007 & 0 & 0.0911 \\ -0.0009 & 0 & \mathbf{[26.4984]} & 0 & -0.0882 & 0 \\ 0 & -1.8007 & 0 & \mathbf{[62.9894]} & 0 & -0.0020 \\ 0.0018 & 0 & -0.0882 & 0 & 0.1792 & 0 \\ 0 & 0.0911 & 0 & -0.0020 & 0 & 0.1851 \end{bmatrix}. \quad \text{(C.5)}$$

From the highlighted diagonal compliance entries [elements (2, 2), (3, 3) and (4, 4)] in Eq. (C.5), the spatial TBM with length error can still be regarded as a 3-DOF planar motion module. However, it shows performance characteristics different from those shown in Eq. (9). For instance, a transverse force along the Y-axis will result in a slight torsion [see element (4, 2)], and a torsional moment will cause a slight transverse displacement along the Y-axis [see element (2, 4)].

References

[1] Lobontiu, N., 2002, *Compliant Mechanisms: Design of Flexure Hinges*, CRC Press, Boca Raton.

[2] Howell, L.L., 2001, *Compliant Mechanisms*, Wiley, New York.

[3] Merlet, J.P., 2006, *Parallel Robotics*, Springer, Berlin.

[4] Kong, X., and Gosselin, C.M., 2007, *Type Synthesis of Parallel Mechanisms*, Springer, Berlin.

[5] Awtar, S., 2004, "*Analysis and Synthesis of Planer Kinematic XY Mechanisms*", Sc.D. thesis, Massachusetts Institute of Technology, Cambridge, MA.

[6] Kota, S., Lu, K.-J., Kreiner, Z., and et al, 2005, "Design and Application of Compliant Mechanisms for Surgical Tools", *Journal of Biomechanical Engineering*, Vol. **127**(6): 981-989.

[7] Krishnan, G., and Ananthasuresh, G. K., 2008, "Evaluation and Design of Displacement-Amplifying Compliant Mechanisms for Sensor Applications", *Journal of Mechanical Design*, Vol. **130**(10): 102304.

[8] Li, J., 2004, "*Electrostatic Zipping Actuators and Their Application to MEMS*", Sc.D. thesis, Massachusetts Institute of Technology, Cambridge, MA.

[9] Zubir, M.N.M., Shirinzadeh, B., and et al, 2009, "A New Design of Piezoelectric Driven Compliant-Based Microgripper for Micromanipulation", *Mechanism and Machine Theory*, Vol. **44**(7): 2248–2264.

[10] Lu, K.-J., and Kota, S., 2003, "Design of Compliant Mechanisms for Morphing Structural Shapes", *Journal of Intelligent Material Systems and Structures*, Vol. **14**(6):379-391.

[11] Howell, L. L., and Midha, A., 1995, "Determination of the Degrees of Freedom of Compliant Mechanisms Using the Pseudo-Rigid-Body Model Concept", *Proceedings of the Ninth World Congress on the Theory of Machines and Mechanisms*, Milano, Italy, Vol. 2:1537-1541.

[12] Yu J.J., Bi S.S., and Zong G.H., Dai J.S., Liu X.J., 2006, "Mobility Characteristics of a Flexure-Based Compliant Manipulator with Three Legs", *Proceedings of the 2006 IEEE/RSJ International Conference on Intelligent Robots and Systems*, Beijing, 1076-1081.

[13] Dai, J. S., and Ding, X. L., 2006, "Compliance Analysis of a Three-Legged Rigidly-Connected Platform Device", *Journal of Mechanical Design*, Vol. **128**(6): 755-764.

[14] Blanding, D. K., 1999, *Exact Constraint: Machine Design Using Kinematic Principles*, ASME, New York.

[15] Su, H.-J., Dorozhkin, D. V., and Vance, J. M., 2009, "A Screw Theory Approach for the Conceptual Design of Flexible Joints for Compliant Mechanisms", *Journal of Mechanisms and Robotics*, Vol. **1**(4): 041009.

[16] Hopkins, J. B., and Culpepper, M. L., 2010, "Synthesis of Multi-Degree of Freedom, Parallel Flexure System Concepts via Freedom and Constraint Topology (FACT). Part I: Principles", *Precision Engineering*, Vol. **34** (1): 259-270.

[17] Hopkins, J. B., and Culpepper, M. L., 2010, "Synthesis of Multi-Degree of Freedom, Parallel Flexure System Concepts via Freedom and Constraint Topology (FACT). Part II: Practice", *Precision Engineering*, Vol. **34** (1): 271-278.

[18] Awtar, S., and Slocum, A. H., 2007, "Constraint-Based Design of Parallel Kinematic XY Flexure Mechanisms", *Journal of Mechanical Design*, Vol. **129**(8): 816-830.

[19] Awtar, S., and Slocum, A. H., 2007, "Characteristics of Beam-Based Flexure Modules", *Journal of Mechanical Design*, Vol. **129** (6): 624-639.

[20] Awtar, S., and Sen, S., 2010, "A Generalized Constraint Model for Two-Dimensional Beam Flexures: Nonlinear Load-Displacement Formulation", *Journal of Mechanical Design*, Vol. **132**(8): 081008.

[21] Hao, G., Kong, X., and Meng, Q., 2010, "Design and Modelling of Spatial Compliant Parallel Mechanisms for Large Range of Translation", *Proceedings of 2010 ASME International Design Engineering Technical Conferences& Computers and Information in Engineering Conference*, Montréal, Québec, Canada, Aug. 15-18. DETC2010-28046.

[22] Hao, G., and Kong, X., 2010, "Novel XY Compliant Parallel Manipulators for Large Displacement Translation with Enhanced Stiffness", *Proceedings of 2010 ASME International Design Engineering Technical Conferences& Computers and Information in Engineering Conference*, Montréal, Québec, Canada, Aug. 15-18. DETC2010-28141
[23] Zelenika, S., and De Bona, F., 2002, "Analytical and Experimental Characterization of High-Precision Flexural Pivots Subjected to Lateral Loads", *Precision Engineering*, Vol. **26**: 381-388.
[24] Angeles J., 2006, "Is There a Characteristic Length of a Rigid-Body Displacement", *Mechanism and Machine Theory*, Vol. **41** (8): 884-896.
[25] Hao, G., 2011, "*Creative Design and Modelling of Large-Range Translational Compliant Parallel Manipulators*", PhD Thesis, Heriot-Watt University, Edinburgh, UK.
[26] Hopkins, J.B., 2010, "*Design of Flexure-Based Motion Stages for Mechatronic Systems via Freedom, Actuation and Constraint Topologies (FACT)*", Ph.D. thesis. Massachusetts Institute of Technology.
[27] Hao, G., Kong, X., and Reuben, R.L., 2011, "A Nonlinear Analysis of Spatial Compliant Parallel Modules: Multi-beam Modules", *Mechanism and Machine Theory*, Vol. **46**(5): 680-706.
[28] Su, H.-J., and Tari, H., 2010, "Realizing Orthogonal Motions with Wire Flexures Connected in Parallel", *Proceedings of 2010 ASME International Design Engineering Technical Conferences& Computers and Information in Engineering Conference, Montréal, Québec, Canada, Aug. 15-18*. DETC2010-28517
[29] Pham, H.-H., and Chen, I.-M., 2005, "Stiffness Modeling of Flexure Parallel Mechanism", *Precision Engineering*, Vol. **29**: 467-478.
[30] Kuipers, J. B., 2002, *Quaternions and Rotation Sequences*, Princeton University Press, US.
[31] Samuel, H. D., and Sergio, N. S., 1979, *Compliant Assembly System*, United States patent, No.: 4155169.
[32] Zhao, H., and Bi, S., 2010, "Accuracy Characteristics of the Generalized Cross-Spring Pivot", *Mechanism and Machine Theory*, Vol. **45**(10): 1434-1448.
[33] Timoshenko, S., and Goodier, J.N., 1951, *Theory of Elasticity*, McGraw-Hill, New York.

List of figures

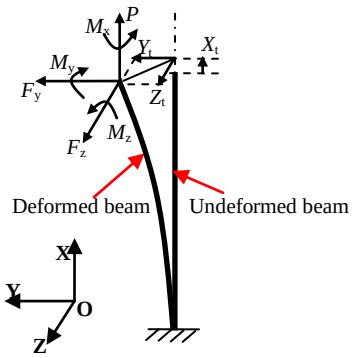

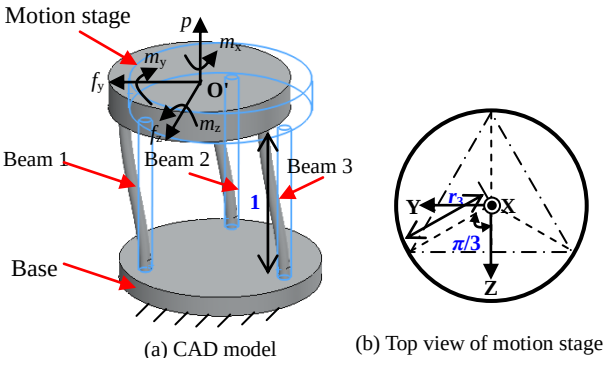

(a) CAD model (b) Top view of motion stage

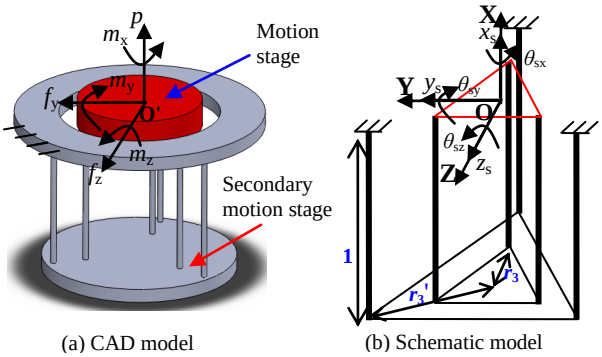

(a) CAD model (b) Schematic model

Figure 4. A spatial tilted TBM

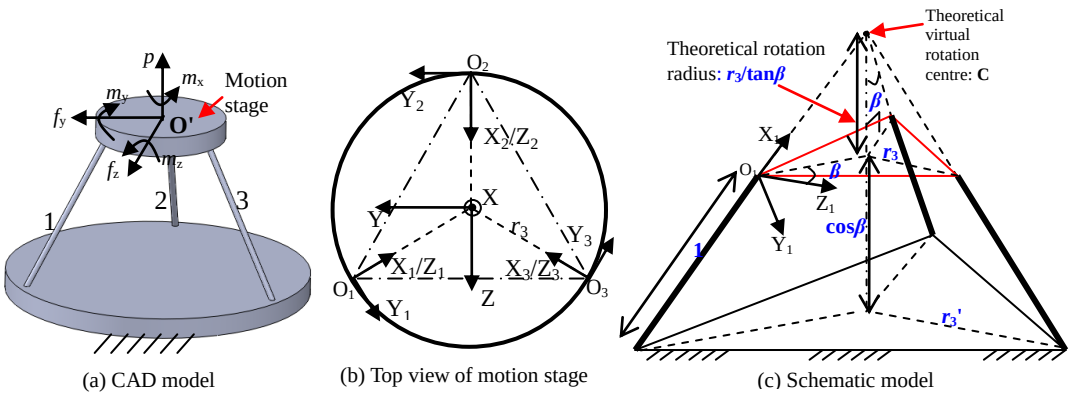

(a) CAD model (b) Top view of motion stage (c) Schematic model

Figure 5. Illustration for real screw axes and theoretical screw axes

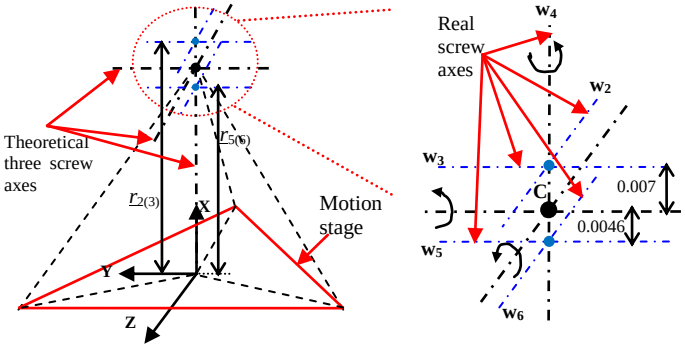

Figure 6. An inverted spatial tilted TBM

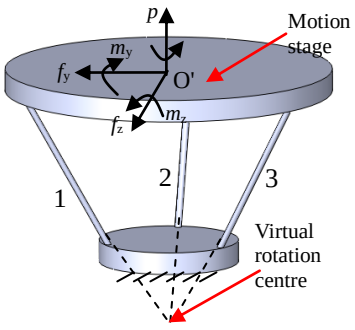

Figure 7. A spatial double tilted TBM

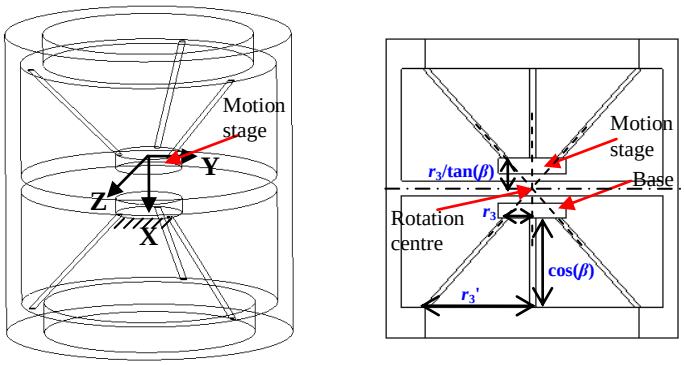

(a) 3-D view of CAD model (b) Front view of CAD model

Figure 8. A spatial double tilted four-beam module

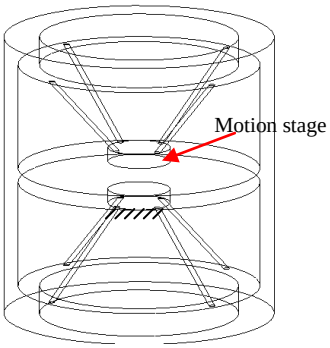

Figure A.1. Parallelogram module with two sheets

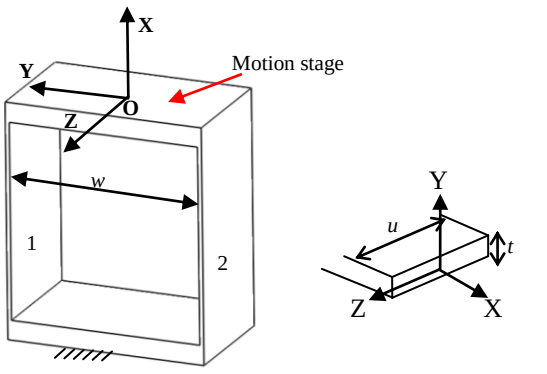

(a) 3-D view of CAD model (b) Dimension of a sheet

Figure B.1. Four-sheet rotational module

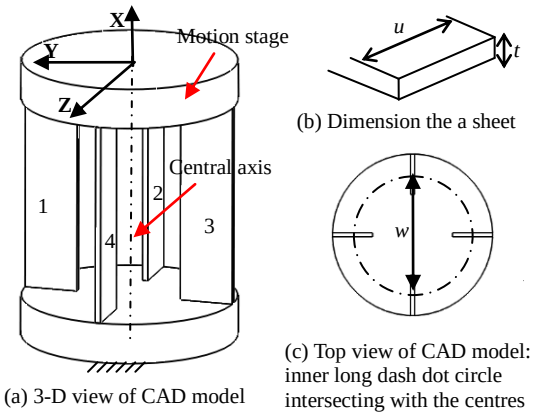

(a) 3-D view of CAD model

(b) Dimension the a sheet

(c) Top view of CAD model: inner long dash dot circle intersecting with the centres

Figure B.2. Double four-sheet rotational modules: a) eight sheets distributed along two circles (largely eliminating the parasitic axial translation accompanying the primary torsion), and b) eight sheets distributed along one circle (completely eliminating the parasitic axial translation accompanying the primary torsion)

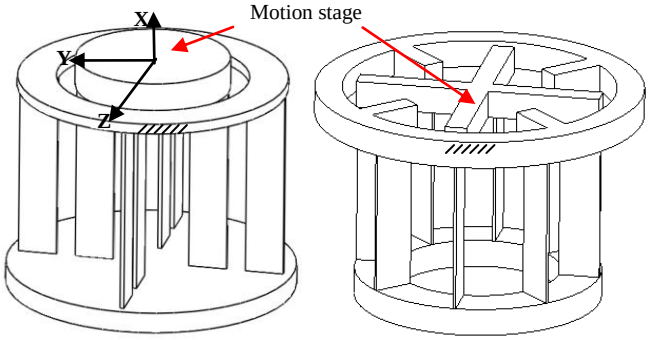

a) Type 1

b) Type 2

Figure C.1. Variation of the spatial TBM